Research Square

Preprints are preliminary reports that have not undergone peer review.
They should not be considered conclusive, used to inform clinical practice,
or referenced by the media as validated information.

PH_3 and AsH_3 Adsorption Through Pristine and Stone-Wales Defected Zinc Oxide Nanosheets: A Density Functional Theory Study

Mohammad Reza Poor Heravi (poorheravi.mr@gmail.com)
Payame Noor University

Research Article

Keywords: Sensor, Density functional theory, Nanostructure, ZnO nanosheet, Arsine, Phosphine

Posted Date: September 27th, 2021

DOI: https://doi.org/10.21203/rs.3.rs-896687/v1

License: This work is licensed under a Creative Commons Attribution 4.0 International License.
Read Full License

Abstract

The adsorption of the XH_3 (X = As or P) molecules were explored onto a pure and Stone-wales defected ZnONS (SW ZnONS) through density functional theory computations. As XH_3 approaches the pure ZnONS their adsorption releases -3.7 to -7.6 kcal/mol, indicating a physisorption. Also, the electronic properties of the nanosheet do not change significantly. But when AsH_3 approaches SW ZnONS, its adsorption releases -23.3 kcal/mol, and electronic analysis showed that the SW ZnONS HOMO/LUMO gap reduces about ~ -27.1% and the electrical conductivity increases significantly. Therefore, the SW ZnONS can generate electrical signals when the AsH_3 molecule approaches, being a hopeful sensor. τ value which calculated for the desorption of AsH_3 from the surface of the SW ZnONS is 9.5 *s*. This indicates that the SW ZnONS has the advantage of having a short τ as a sensor for AsH_3 detection.

1. Introduction

Arsine (AsH_3) has many applications in various fields. For example, it is used in the solid-state lasers and synthesis of semiconducting materials. It is also applied to make GaAs semiconductors with chemical vapor deposition at 700–900°C [1]. AsH_3 is the strongest hemolytic toxin found in industry. This substance is flammable and is very toxic if inhaled. Short-term exposure to a small amount of arsenic can cause death or permanent injury [2]. Therefore, it is very important to identify this gas, which has rarely been addressed. The large surface area of nanostructures is highly susceptible to the adsorption of gas molecules, for example, the graphene has been used as a sensor to adsorb many hazardous gases [3].

Phosphine (PH3) is a highly toxic, flammable, colorless gas that is classified as a pnictogen hydride. It can be absorbed through the skin or by inhalation [4]. As a respiratory toxin, it affects the transport of oxygen or interferes with the use of oxygen by various cells in the body [5]. Exposure leads to pulmonary edema (the lungs fill with fluid) [6]. PH3 gas is heavier than air, so it is closer to the floor [7]. It seems that this substance is mainly an oxidative oxidation toxin that causes cell damage by stimulating oxidative stress and mitochondrial dysfunction [8, 9]. It is very important to develop suitable measuring materials for PH3 gas. Ms. Shahzad Khan's research shows that zinc sulfide nanotubes are sensitive to phosphine [10]. V2O5 (001) is also a good candidate as a hazardous gas nanosensor [11]. The first graphene-based ammonia gas sensor was reported by Andre Game Group in 2007 using a micro-mechanical cutter of graphite on an oxidized silicon layer [12]. However, the interaction of most chemicals with the surface of various nanostructures is weak.

Nowadays, the use of metal oxide-based sensors has attracted a lot of attention due to their compact size, simple electronic measuring devices, easy and cost-effective production [13–20]. Zinc oxide is one of the most widely used experimental materials due to its excellent photon properties, high excitation energy, and superior electronic properties. [21–24]. Zinc oxide nanostructures with different morphologies have already been produced, such as nanotubes, nanosheets, nanowires, etc. [25–28]. However, structure

and morphology may affect the sensory properties of nanostructures [28–31]. Among these nanomaterials, ZnO (ZnONS) nanoparticles have been shown to have promising measurement properties due to their higher surface-to-volume ratio, superior electronic properties, and additional active sites [32].

However, pure ZnONS have a rather poor interaction with many chemical and biological agents. To improve the performance of nanostructures, some methods are accessible such as impurity atom doping or decoration, chemical functionalization, structural defect creation, etc. [33–38]. Stone-Wales defected (SW) on the surface of zinc oxide is a good way to increase their sensing performances. Ahangari et al. have presented that the sensing performance of the zinc oxide nanomaterial upsurges meaningfully by various defects [39]. Chen et al. have demonstrated that the SW is an appropriate technique for increased sensitivity. [40]. Consequently, the ZnONS may be a promising choice for probable requests. The aim of this manuscript is to inspect the XH_3 (X = P or As) adsorption onto pure and SW ZnONS to find a new way to identify this gas by density functional theory (DFT) calculations.

2. Computational Methods

A 103-zinc and 103-oxygen ZnONS was selected as an adsorbent for XH_3 and it end atoms were saturated by H atoms for reducing the boundary effects. Energy computations, optimization of geometry, and analysis of state density were carried out on the pure and SW sheets using the dispersion augmented B3LYP, i.e, *B3LYP-D.* Here, Grimme's “D” term is used for evaluating dispersion forces. As a basis set, 6-311G** (d) was employed and all of the computations were performed by employing GAMESS software [41]. GaussSum [42] software was employed for drawing the density of states (DOS) diagrams. According to previously carried out studies, B3LYP has been used for nanostructures due to its high performance [43–46].

Following the adsorption of the XH_3 molecules on the pure as well as SW ZnONS, its energy of adsorption is computed as follows:

$$E_{ad} = E(XH_3/sheet) - E(XH_3) - E(sheet) + E_{BSSE} \quad (1)$$

Here, E(sheet) is pure or SW sheet energy, $E(XH_3)$ is the XH_3 molecules energy, $E(XH_3/sheet)$ is the energy of the sheet that adsorbed the XH_3 molecules. For the structures under study, the negative energy of adsorption shows the exothermic nature of this adsorption. The basis set superposition error is corrected for interactions. The HOMO-LUMO energy gap, which is indicated by E_g, was calculated as below:

$$E_g = E_{LUMO}-E_{HOMO} \quad (2)$$

Here, E_{HOMO} and E_{LUMO} designate the energy of the highest occupied and the lowest unoccupied molecular orbitals, respectively.

3. Results And Discussion

3.1. Pure ZnONS

We displayed the geometry of optimized ZnONS in Fig. 1. Zn–O is predicted in the structure of the sheet with lengths of 1.95 Å. From DOS plot in Fig. 1, it is seen that the E_g between the LUMO and HOMO of the pure ZnONS is about 3.81 eV, indicating a semiconducting property. In order to find the most stable complex of XH_3/ZnONS, we considered various primary adsorption geometries. Figures 2 and 3 show the four most stable states. In complex **A** and **C**, the molecules is adsorbed almost in parallel with the ZnONS surface. In configuration **A** and **C**, the XH_3 approaches to the one X and one H atoms through the Zn and O atoms, and in configuration **B** and **D**, the XH_3 interacts with one X atom through the Zn atom on the sheet.

Configuration **B** and **D** indicate a poor interaction between the ZnONS surface and XH_3 (Figs. 2 and 3) and the E_{ad} are − 4.5 and − 7.6 kcal/mol, respectively. They indicate the physical nature of these interaction, which are stronger than the configuration **A** and **C**, respectively. It should be noted that the weak interaction in complexes **A** and **C** compared to **B** and **D** is the higher strain and steric effect when the X and H atoms simultaneously react with the surface of the sheet. By the adsorption of XH_3, there is a slight change in both conduction and valence levels, which causes a decrease in E_g of the complex from 3.81 eV in the pure ZnONS to 3.52, 3.49, 3.41 and 3.33 eV for **A**, **B**, **C** and **D** complexes, respectively. Thus, the adsorption of XH_3 on the pure ZnONS is a physisorption process. The electrical conductivity of the nanosheet can change because of the change of E_g based on the equation below:

$$\sigma = AT^{3/2}e^{(-\frac{E_g}{2kT})} \quad (3)$$

Here, k designates the Boltzmann constant and σ is the electrical conductivity and A designates a constant (electrons/$m^3K^{3/2}$)[47]. At a constant temperature, as the amount of E_g gets lower, the electrical conductivity becomes higher. So, the electrical conductivity of ZnONS increases significantly following a decrease in E_g, which is caused by the adsorption process. Therefore, this change of E_g is very small and negligible which cannot generate a proper electronic noise to detect the presence of XH_3 gases. Thus, pure ZnONS cannot be a proper sensor for XH_3 detection.

3.2. XH_3 adsorption on the SW ZnONS

The typical topological defect in nanostructures is the SW defect which consists of seven-membered and two pairs of five-membered rings. The SW defects are made by rotating the bond 90◦. SW is obtained by rotating a Zn-O bond on the pure ZnONS. The atomic configuration for the SW defect in ZnONS is shown in Fig. 4. From DOS plot in Fig. 4, it is seen that the E_g between the LUMO and HOMO of the SW ZnONS is about 3.24 eV, indicating a semiconducting property.

The interaction of a SW ZnONS with an XH_3 molecules will be investigated. Here, the adsorption of XH_3 is inspected on the SW ZnONS. For this purpose, the XH_3 molecules are located in above SW sites on the

SW ZnONS surface such as the over the center of a five, six and seven-membered ring, top of the bond bridge and on the O or Zn atom. Totally, the XH_3 are located in parallel with the surface of SW ZnONS or perpendicular to it. Two local minima is predicted for each XH_3 after the optimization process (Figs. 5 and 6). In configuration **I**, the PH_3 interacts by its one P and one H atoms with one Zn and O atoms of the defected site SW ZnONS. Moreover, the corresponding interaction distances between the Zn and O atoms of defected sheet and the P and H atoms of the complex **I** is about 2.98 and 3.11 Å, respectively, and an E_{ad} is about − 12.1 kcal/mol (Table 2). In configuration **II (**Fig. 5**)**, the PH_3 interacts by its one P atom with one Zn atom of the defected site SW ZnONS with distance 2.77 Å, and an E_{ad} is about − 13.4 kcal/mol (Table 2). According Eq. 3, the adsorption of PH_3 on the SW ZnONS is a physisorption process and SW ZnONS cannot detect PH_3 gas. Therefore SW ZnONS isn't a sensor for PH_3 gas.

Table 1
Adsorption energy (Ead, kcal/mol) for PH_3 and AsH_3 adsorption on the pristine ZnO nanosheet (Figs. 2 and 3). Energy of HOMO, LUMO, and HOMO-LUMO energy gap (E_g) in eV. The ΔE_g indicates the change of E_g after the adsorption process. Work function (Φ) for Pristine ZnO nanosheet

Structure	E_{ad}	E_{HOMO}	E_F	E_{LUMO}	E_g	ΔE_g(%)	Φ	%ΔΦ
ZnONS	-	-6.36	-4.46	-2.55	3.81	-	4.46	-
A	-3.7	-6.04	-4.28	-2.52	3.52	-7.6	4.28	-3.9
B	-4.5	-5.98	-4.24	-2.49	3.49	-8.4	4.24	-5.0
C	-6.7	-5.89	-4.19	-2.48	3.41	-10.5	4.19	-6.2
D	-7.6	-5.80	-4.14	-2.47	3.33	-12.6	4.14	-7.3

Table 2
Adsorption energy (E_{ad}, kcal/mol) for PH_3 and AsH_3 adsorption on the Stone-Wales ZnO nanosheet (SW ZnONS). Energy of HOMO, LUMO, and HOMO-LUMO energy gap (E_g) in eV. The ΔE_g indicates the change of E_g after the adsorption process. Work function (Φ) for SW ZnONS (Figs. 5 and 6).

Structure	E_{ad}	E_{HOMO}	E_F	E_{LUMO}	E_g	ΔE_g(%)	Φ	%ΔΦ
SW ZnONS	-	-5.76	-4.14	-2.51	3.25	-	4.14	-
I	-12.1	-5.32	-3.91	-2.49	2.83	-12.9	3.91	-5.6
II	-13.4	-5.24	-3.86	-2.47	2.77	-14.8	3.86	-6.9
III	-18.5	-4.97	-3.71	-2.45	2.52	-22.5	3.71	-10.4
IV	-23.3	-4.81	-3.63	-2.44	2.37	-27.1	3.63	-12.4

In configuration **III**, the AsH_3 approaches to one Zn and one O atoms with an interacting distance of 2.82 Å for Zn…As and 2.64 Å for H…O. In configuration **IV**, the AsH_3 interacts with one Zn atom through one of its As atom which the Zn…As distance is about 2.57 Å. For configuration **III**, E_{ad} is -18.5 kcal/mol and it is

-23.3 kcal/mol for configuration **IV** (Table 2 and Fig. 6). It seems that because As atom is larger than P atom, it was able to react better with the SW ZnONS surface. Therefore, the results display that SW defected significantly strengthens the adsorption of AsH_3 on SW ZnONS. The adsorption of XH_3 in the SW ZnONS is more favorable compare to the pure ZnONS, which is due to the fact that the localization of the HOMO is mainly on the defected site in the SW ZnONS (Fig. 7).

As shown in Fig. 8 (configuration **IV**), the partial DOS plot illustrates that a new occupied orbital appears on the SW ZnONS electron forbidden area (E_g) at -2.81 eV due to the presence of AsH_3. The HOMO profile shown in Fig. 8 also confirms that the HOMO of complex shifts on the AsH_3 with changing the HOMO energy. The E_g of SW ZnONS decreases significantly, following the adsorption of AsH_3 and the sheet becomes more conductive. Numerically, its E_g in complex **IV** decreased from 3.25 to 2.37 eV (by approximately − 27.1%). According to Eq. 3, the SW ZnONS sensitivity toward the AsH_3 molecule increase. Thus, it was found that SW ZnONS can selectively detect AsH_3 molecule.

To further evaluate the sensitivity of the surfaces, the changes in the work function (Φ) were investigated before and following the adsorption process. Φ of a semiconductor is the least amount of work needed for the extraction of an electron from the Fermi level. The re-examination of the gas-induced Φ by the suspended amplitude effect modifiers has been accepted for many years as the basis for realizing sensor operating systems [48]. Theoretically, in vacuum, the released electron current density is defined as follows:

$$j = AT^2 exp\left(\frac{-\Phi}{kT}\right) \quad (4)$$

Where, T is the temperature in Kelvin, A is the Richardson constant in A/m^2 and Φ is the work function. Φ was computed as follows:

$$\Phi = E_{inf} - E_F \quad (5)$$

Where E_F is the energy of Fermi level and E_{inf} is the electrostatic potential, which is supposed to be equal to 0 at infinity. Φ of the sheet was subtracted from that of the complexes and obtained Φ changes (ΔΦ). Φ for pristine ZnONS was about 4.46 eV and changed very slightly after adsorbing the XH_3 molecules, which can be ignored. But when AsH_3 is adsorbed onto SW ZnONS (configuration **IV**), Φ is significantly reduced from 4.14 to 3.63 eV. According to Eq. 4, the emitted current density and Φ are exponentially related to each other. Therefore, it can be said that after the adsorption of AsH_3, by decreasing the Φ, the current density of the emitted electron increases dramatically. Accordingly, we think that SW defected in ZnO is a hopeful way to increase the sensitivity of ZnONS toward AsH_3 which pristine ZnONS did not.

3.3. Recovery time

An important factor which should be taking into account in the development of sensors is the strength of interactions. A higher recovery time is obtained if E_{ad} gets more negative:

$$\tau = {v_0}^{-1} exp^{(-\frac{E_{ad}}{kT})} \quad (6)$$

Here, T is the temperature, v_0 is the attempt frequency, and k shows the Boltzmann's constant which is ~ $2.0 \cdot 10^{-3}$ kcal/mol.K. At 298 K and the ultra-violet light (υ ~ 10^{16} s^{-1}), τ for the desorption of AsH_3 from the SW ZnONS surface is computed to be 9.5 *s*, which indicates the nanosheet has a short τ as a sensor for the detection of AsH_3. For the sake of comparison, τ value have been provided for different chemical agents, inclufing SO_2/Al-doped *h*-BN [49], adrucil/Si-doped phagraphene [50], metronidazole/B_{36} borophene [51], phosgene/BN nanocones-180 [52], and cathinone/$B_{12}N_{12}$ [53], which is 27.6, 0.02, 1.53, 0.48, and 0.54 s, respectively.

4. Conclusions

We scrutinized the adsorption of the XH_3 molecules onto the pure and SW ZnONS by performing DFT computations. It was revealed that the XH_3 molecules have weak adsorption on the pristine ZnONS with low E_{ad} and much interaction distance. The electronic properties of the pristine ZnONS changed slightly following the adsorption of XH_3. However, the interaction of the AsH_3 gas the SW ZnONS was strong. In the most stable AsH_3/SW ZnONS complex, the adsorption of AsH_3 was onto the nanosheet surface via its one As atom and E_{ad} was − 23.3 kcal/mol. The HOMO level of the SW ZnONS was destabilized to a great extent following the adsorption of AsH_3. Therefore, there was a considerable reduction in its E_g, thereby increasing its electrical conductivity. The results suggest that SW defected the ZnONS may be a hopeful way for increasing its sensitivity to AsH_3 significantly. τ value which calculated for the desorption of AsH_3 from the surface of the SW ZnONS is 9.5 *s*. This indicates that the SW ZnONS has the advantage of having a short τ as a sensor for AsH_3 detection.

Declarations

Funding: Not applicable

Conflicts of interest/Competing interests: There is no conflict of interest

Availability of data and material: All data will be available if required.

Code availability: Not applicable

Authors' contributions: Not applicable

Ethics approval: We approved all Ethics

Consent to participate: Not applicable

Consent for publication: Not applicable

Availability of data and material: Not applicable

Authors' contributions: Not applicable

References

1. Scheele CW, Hermbstädt SF, Carl Wilhelm Scheele) Sändig, 1971
2. Environmental U, Protection Agency. 1992, Superfund Engineering Issue ~ Treatment of Lead-Contaminated Soils. EPA/540/2–91/009. Office of Solid Waste and Emergency Response. Washington, DC. and Office of Research and Development, Risk Reduction Engineering Laboratory. Cincinnati, Ohio, (1990)
3. Rastegar SF, Peyghan AA, Hadipour NL (2013) Response of Si-and Al-doped graphenes toward HCN: a computational study. Applied surface science 265:412–417
4. Lee B-H, Lee S-E, Annis PC, Pratt SJ, Park B-S, Tumaalii F (2002) Fumigant toxicity of essential oils and monoterpenes against the red flour beetle, Tribolium castaneum Herbst. Journal of Asia-Pacific Entomology 5:237–240
5. Bhuvaneswari R, Nagarajan V, Chandiramouli R (2019) Arsenene nanoribbons for sensing NH3 and PH3 gas molecules–a first-principles perspective. Appl Surf Sci 469:173–180
6. Kuimov VA, Matveeva EA, Khutsishvili SS, Vakul'skaya TI, Sinegovskaya LM, Malysheva SF, Gusarova NK, Trofimov BA (2017) Reaction of 1-bromonaphthalene with PH3 in the t-BuOK/DMSO system: PCl3-free synthesis of di (1-naphthyl) phosphine and its oxide. Tetrahedron 73:4723–4729
7. Simpson JE (1982) Gravity currents in the laboratory, atmosphere, and ocean. Annu Rev Fluid Mech 14:213–234
8. Sebbane YB (2011) Lighter than air robots: guidance and control of autonomous airships. Springer Science & Business Media
9. Kreitler CW (1975) Determining the source of nitrate in ground water by nitrogen isotope studies. Virtual Landscapes of Texas
10. Khan MS, Srivastava A, Chaurasiya R, Khan MS, Dua P (2015) NH3 and PH3 adsorption through single walled ZnS nanotube: first principle insight. Chem Phys Lett 636:103–109
11. Víctor AR, Pablo LDQ, Nahuel MY, General adsorption model for H2S, H2Se, H2Te, NH3, PH3, AsH3 and SbH3 on the V2O5(001) surface including the van der Waals interaction, Chem. Phys. Lett. 720 (2019) 58–63
12. Schedin F, Geim AK, Morozov SV, Hill EW, Blake P, Katsnelson MI, Novoselov KS (2007) Detection of individual gas molecules adsorbed on graphene. Nat Mater 6:652–655
13. Chaitra U, Muhammed Ali AV, Mahesha MG, Kompa A, Kekuda D (2021) K. Mohan Rao, Property evaluation of spin coated Al doped ZnO thin films and Au/AZO/FTO Schottky diodes. Superlattices Microstruct 155:106903

14. Tan J, Shi F-N, Hu F, Shi G-M, Tian B, You H (2018) Synthesis, crystal structure of a lithium - zinc bimetal coordination polymer and its graphene composite as anode materials for lithium-ion battery. Inorg Chem Commun 91:112–118
15. Kumar P, Dev S, Kumar A, Thakur R, Dhar R (2021) Impact of indium doping on the anti-biofilm activity of ZnO thin films against Escherichia coli and Staphylococcus aureus. Superlattices Microstruct 150:106741
16. Zhou L, Bai J, Liu Y, Liu F, Wang H, Zhang Y, Lu G (2020) Highly sensitive C2H2 gas sensor based on Ag modified ZnO nanorods. Ceram Int 46:15764–15771
17. Chandiramouli R, Sriram S, Balamurugan D (2014) Quantum chemical studies on (ZnO) n/(NiO) n heterostructured nanoclusters. Mol Phys 112:151–164
18. Marinelli F, Grillet Y, Pellenq RJ-M, The adsorption of argon on ZnO at 77 K, Molecular Physics, 97 (1999) 1207–1224. [12] Rafiee Z, Roshan H, Sheikhi MH, Low concentration ethanol sensor based on graphene/ZnO nanowires, Ceramics International, 47 (2021) 5311–5317
19. Wen H, Surface enhancement of Raman and absorption spectra from cyanine dye D266 adsorbed on ZnO colloids, Molecular Physics, 88 (1996) 281–290. [14] Wang X, Li S, Xie L, Li X, Lin D, Zhu Z, Low-temperature and highly sensitivity H2S gas sensor based on ZnO/CuO composite derived from bimetal metal-organic frameworks, Ceramics International, 46 (2020) 15858–15866
20. Zheng W-C, He L, Mei Y, Yang W-Q (2010) Investigations on the g factors of the ground and excited states for Cu2 + ions in ZnO crystal. Mol Phys 108:1583–1588
21. Chen M-Y, Hong Z-H, Fang T-H, Kang S-H (2014) Molecular dynamics simulation of nanoscale mechanical behaviour of ZnO under nanoscratching and nanoindentation. Mol Phys 112:3152–3164
22. Xu C, Song Y, Lu LF, Cheng CW, Liu DF, Fang XH, Chen XY, Zhu XF, Li DD (2013) Electrochemically hydrogenated TiO2 nanotubes with improved photoelectrochemical water splitting performance. Nanoscale Res Lett 8:391
23. Wu H, Xu C, Xu J, Lu LF, Fan ZY, Chen XY, Song Y, Li DD (2013) Enhanced supercapacitance in anodic TiO2 nanotube films by hydrogen plasma treatment. Nanotechnology 24:455401
24. Guan Y, Wang DW, Zhou X, Sun P, Wang HY, Ma J, Lu GY (2014) Hydrothermal preparation and gas sensing properties of Zn-doped SnO2 hierarchical architectures. Sens Actuators B 191:45–52
25. Lu GY, Xu J, Sun JB, Yu YS, Zhang YQ, Liu FM (2012) UV-enhanced room temperature NO2 sensor using ZnO nanorods modified with SnO2 nanoparticles. Sens Actuators B 162:82–88
26. [26] H, Wu DD, Li XF, Zhu CY, Yang DF, Liu XY, Chen Y, Song LF, Lu (2014) High-performance and renewable supercapacitors based on TiO2 nanotube array electrodes treated by an electrochemical doping approach. Electrochim Acta 116:129–136
27. Meng FL, Hou NN, Ge S, Sun B, Jin Z, Shen W, Kong LT, Guo Z, Sun YF, Wu H, Wang C, Li MQ (2015) Flower-like hierarchical structures consisting of porous single-crystalline ZnONs and their gas sensing properties to volatile organic compounds (VOCs). J Alloys Compd 626:124 –130.
28. Song DM, Wang TH, Li JC (2012) First principles study of periodic size dependent band gap variation of Cu doped ZnO single-wall nanotube. J Mol Model 18:5035–5040

29. Wang C, Xu S, Ye L, Lei W, Cui Y (2011) Theoretical investigation of ZnO and its doping clusters. J Mol Model 17:1075–1080
30. Abdulsattar MA (2017) Chlorine gas reaction with ZnO wurtzoid nanocrystals as a function of temperature: a DFT study. J Mol Model 23:125
31. Kaewruksa B, Ruangpornvisuti V (2012) First principles investigation of oxygen adsorptions on hydrogen–terminated ZnO graphene-like nanosheets. J Mol Model 18:1447–1454
32. Srivastava A, Gupta P, Khan MS, Kanoun MB (2018) S. Goumri-Said, Electronic and optical properties of functionalized zigzag ZnO nanotubes. J Mol Model 24:48
33. Wu J-H, Liu S-Y, Li S, Jiang Y-l, Ru G-P, Qu X-P (2012) The influence of ZnO seed layers on n-ZnO nanostructure/p-GaN LEDs. Appl Phys A 109:489–495
34. Zhang H, Sun M, Song L, Guo J, Zhang L (2019) Fate of NaClO and membrane foulants during in-situ cleaning of membrane bioreactors: Combined effect on thermodynamic properties of sludge. Biochemical engineering journal 147:146–152. doi:10.1016/j.bej.2019.04.016
35. Sun M, Yan L, Zhang L, Song L, Guo J, Zhang H (2019) New insights into the rapid formation of initial membrane fouling after in-situ cleaning in a membrane bioreactor. Process biochemistry (1991), 78, 108–113. doi: 10.1016/j.procbio.2019.01.004
36. Zhu J, Yang K, Chen Y, Fan G, Zhang L, Guo B, Zhao R (2021) Revealing the substitution preference of zinc in ordinary Portland cement clinker phases: A study from experiments and DFT calculations. J Hazard Mater 409:124504. doi:10.1016/j.jhazmat.2020.124504
37. Meng F, Zheng H, Sun Y, Li M, Liu J (2017) Trimethylamine sensors based on Au-modified hierarchical porous single-crystalline ZnO nanosheets. Sensors 17:1478
38. Lv J, Gong W, Huang K, Zhu J, Meng F, Song X, Sun Z (2011) Effect of annealing temperature on photocatalytic activity of ZnO thin films prepared by sol–gel method. Superlattices Microstruct 50:98–106
39. Ahangari MG, Mashhadzadeh AH, Fathalian M, Dadrasi A, Rostamiyan Y, Mallahi A (2019) Effect of various defects on mechanical and electronic properties of zinc-oxide graphene-like structure: A DFT study. Vacuum 165:26–34
40. Chen W, Li Y, Yu G, Zhou Z, Chen Z (2009) Electronic structure and reactivity of boron nitride nanoribbons with stone-wales defects. J Chem Theory Comput 5:3088–3095
41. Schmidt MW, Baldridge KK, Boatz JA, Elbert ST, Gordon MS, Jensen JH, Koseki S, Matsunaga N, Nguyen KA, Su S, Windus TL, Dupuis M, Montgomery JA (1993) J Comp Chem 14:1347–1363
42. O'Boyle N, Tenderholt A (2008) K. Langner, cclib: A library for package-independent computational chemistry algorithms. J Comput Chem 29:839–845
43. [1] Y, Burk P, Koppel IA, Koppel I, Leito I, Travnikova O (2000) Critical test of performance of B3LYP functional for prediction of gas-phase acidities and basicities. Chem Phys Lett 323:482–489
44. Paier J, Marsman M, Kresse G (2007) Why does the B3LYP hybrid functional fail for metals? J Chem Phys 127:024103

45. Tirado-Rives J, Jorgensen WL (2008) Performance of B3LYP density functional methods for a large set of organic molecules. J Chem Theory Comput 4:297–306
46. Zhang IY, Wu J, Xu X (2010) Extending the reliability and applicability of B3LYP. Chem Commun 46:3057–3070
47. Dev S, Kumar P, Rani A, Agarwal A, Dhar R, Development of indium doped ZnO thin films for highly sensitive acetylene (C2H2) gas sensing, Superlattices and Microstructures, 145 (2020) 106638.&#8206
48. Stegmeier S, Fleischer M, Hauptmann P (2010) Influence of the morphology of platinum combined with β-Ga2O3 on the VOC response of work function type sensors. Sens Actuators B 148:439–449
49. Hosseinian A, Salary M, Arshadi S, Vessally E, Edjlali L (2018) The interaction of phosgene gas with different BN nanocones: DFT studies. Solid State Commun 269:23–27
50. Nejati K, Hosseinian A, Vessally E, Bekhradnia A, Edjlali L (2017) A comparative DFT study on the interaction of cathinone drug with BN nanotubes, nanocages, and nanosheets. Appl Surf Sci 422:763–768
51. Cossi M, Barone V, Cammi R, Tomasi J (1996) Ab initio study of solvated molecules: a new implementation of the polarizable continuum model. Chem Phys Lett 255:327–335
52. Dang C, Lin Y (2020) Detection of phenol by defective inorganic BN nanosheet: A DFT study. Inorg Chem Commun 117:107977
53. Yulin Z, Shuosi O, Zhao J (2020) Potential application of pristine and Al-doped graphyne-like BN nanosheet for detection of anticancer fluorouracil drug. J Mol Model 26:169

Figures

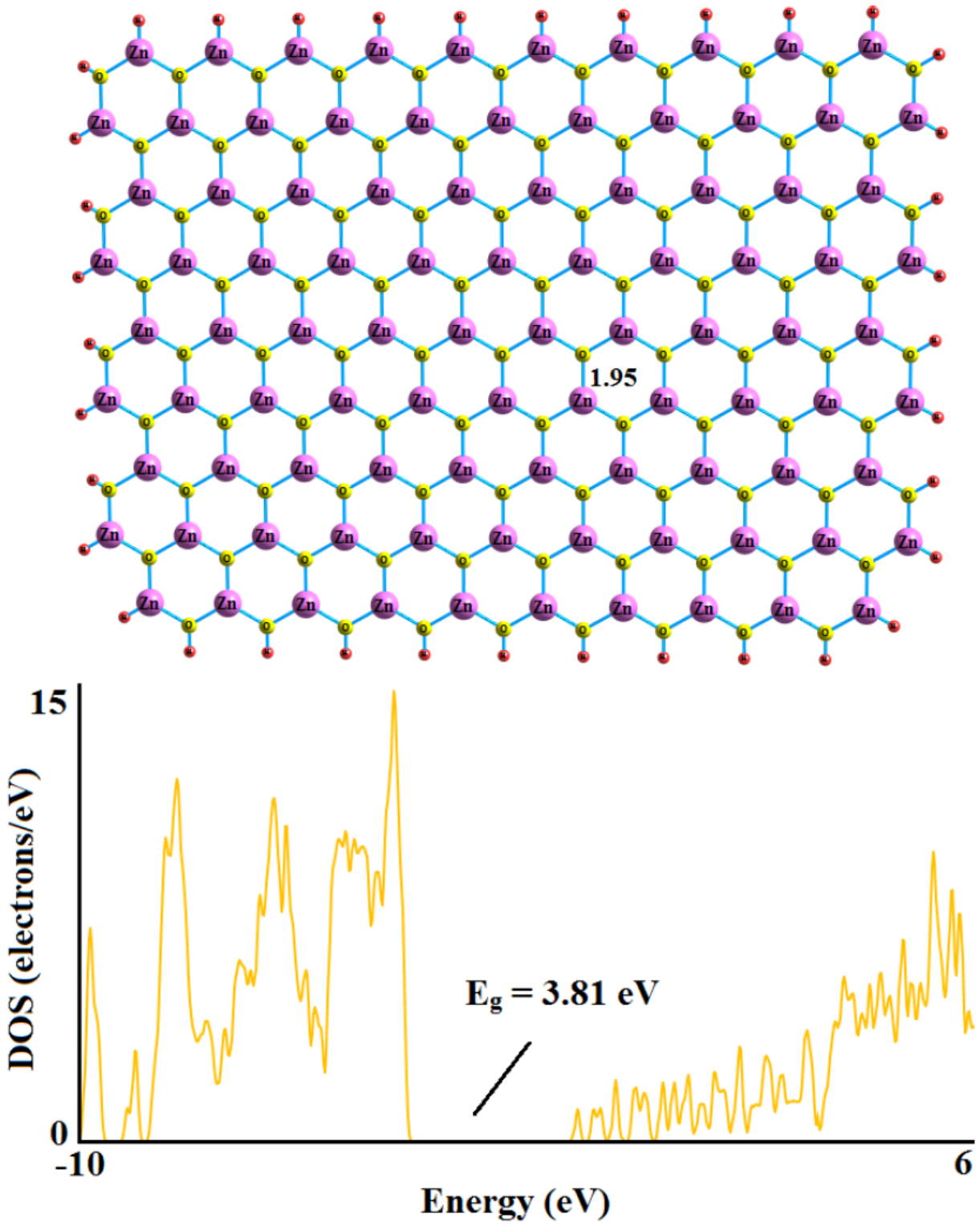

Figure 1

Optimized structure of the ZnO nanosheet and its DOS profile. Distance is in Å.

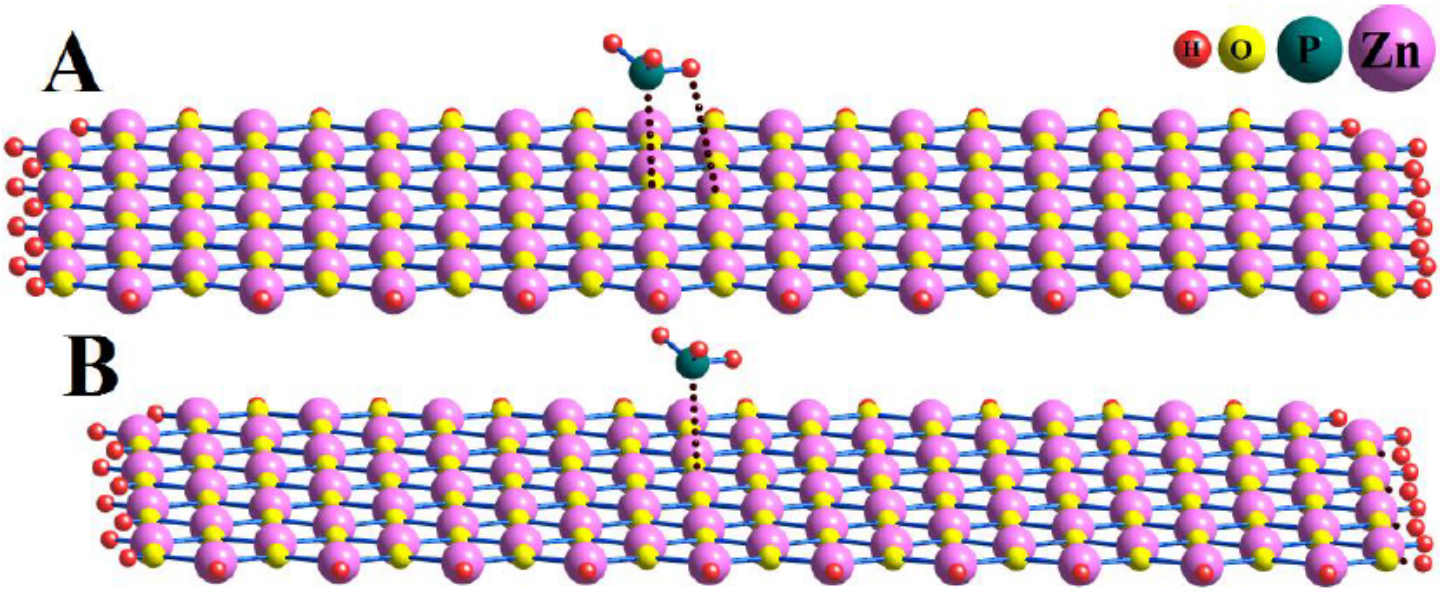

Figure 2

Optimized structure of PH3/ZnO nanosheet complexes.

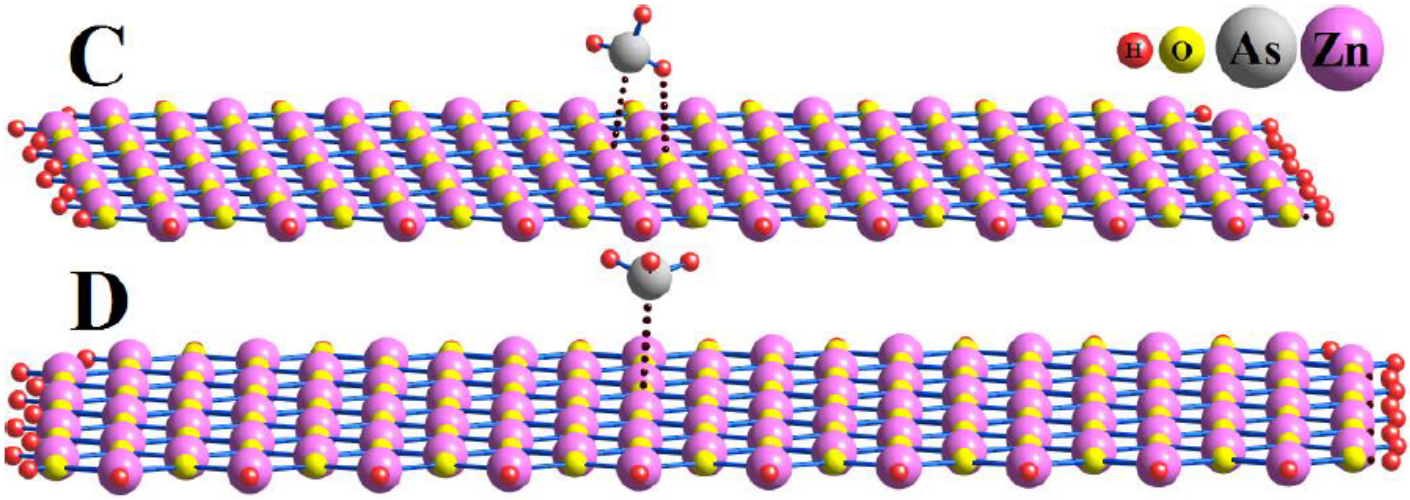

Figure 3

Optimized structures of AsH3/ZnO nanosheet complexes.

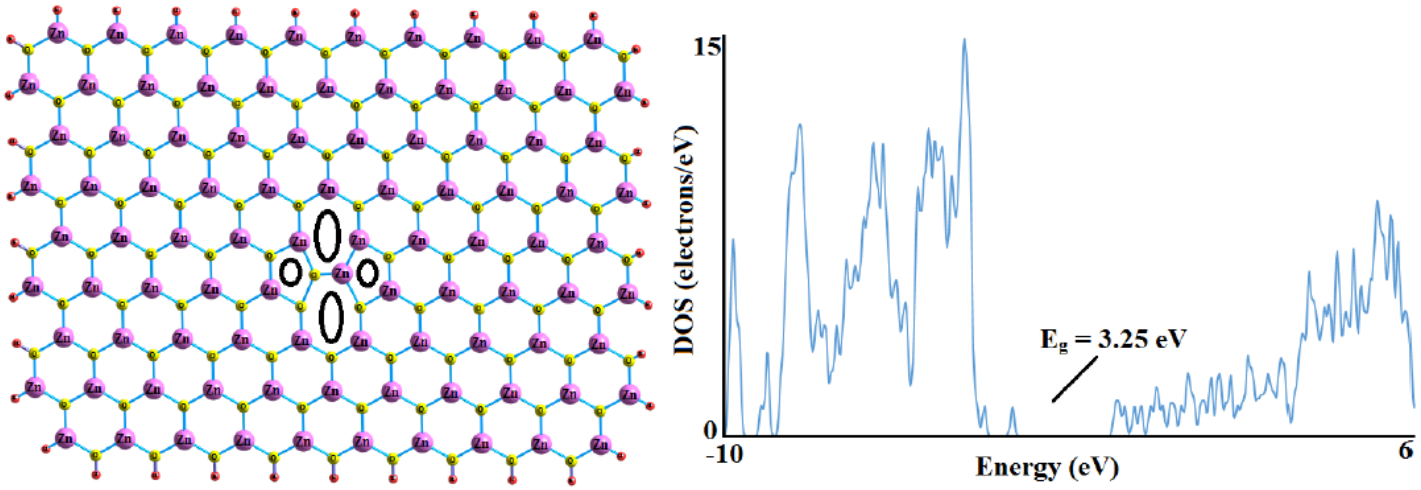

Figure 4

Optimized structure of the Stone-Wales defected ZnO nanosheet and its DOS profile.

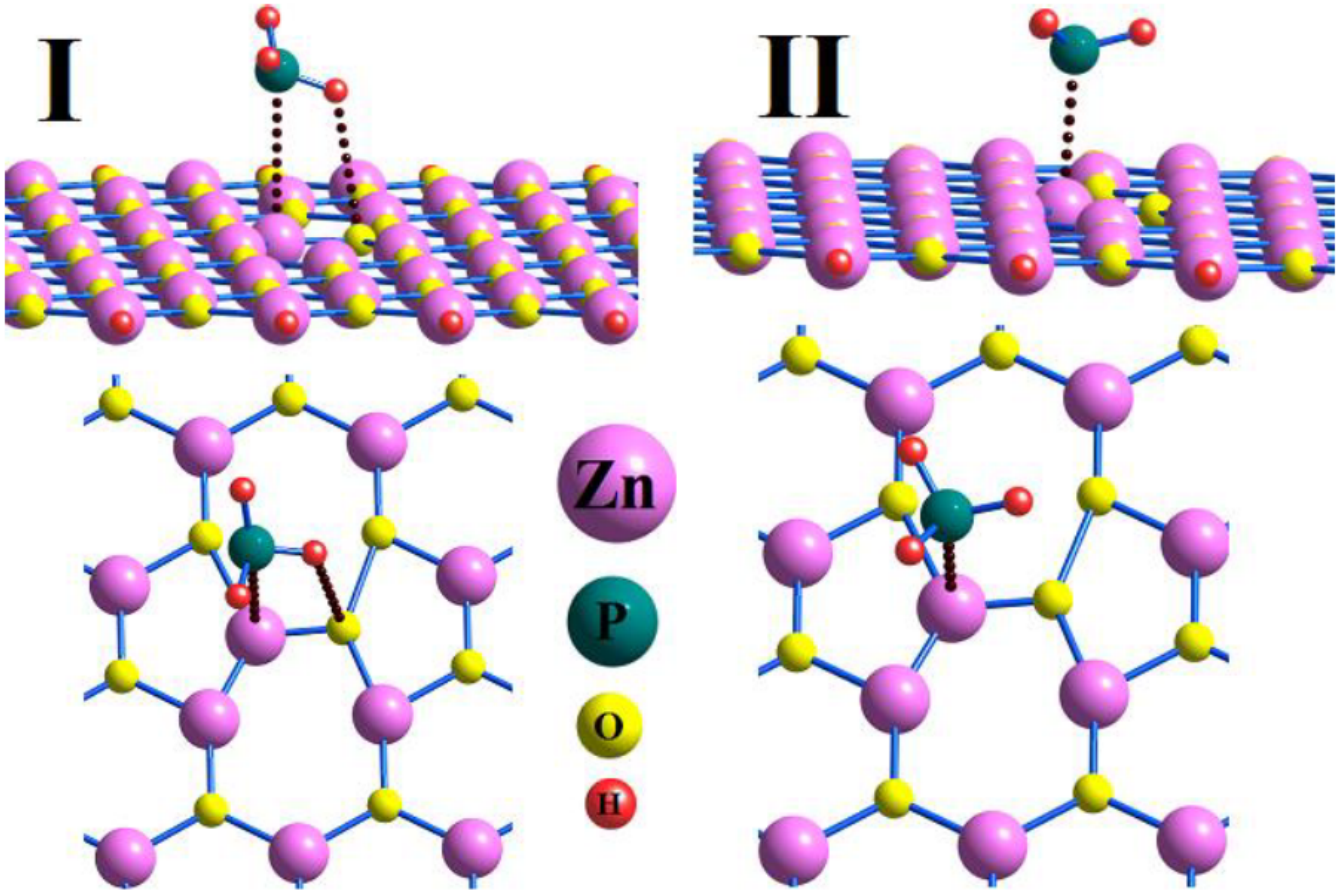

Figure 5

Optimized structure of PH3/SW ZnO nanosheet complexes.

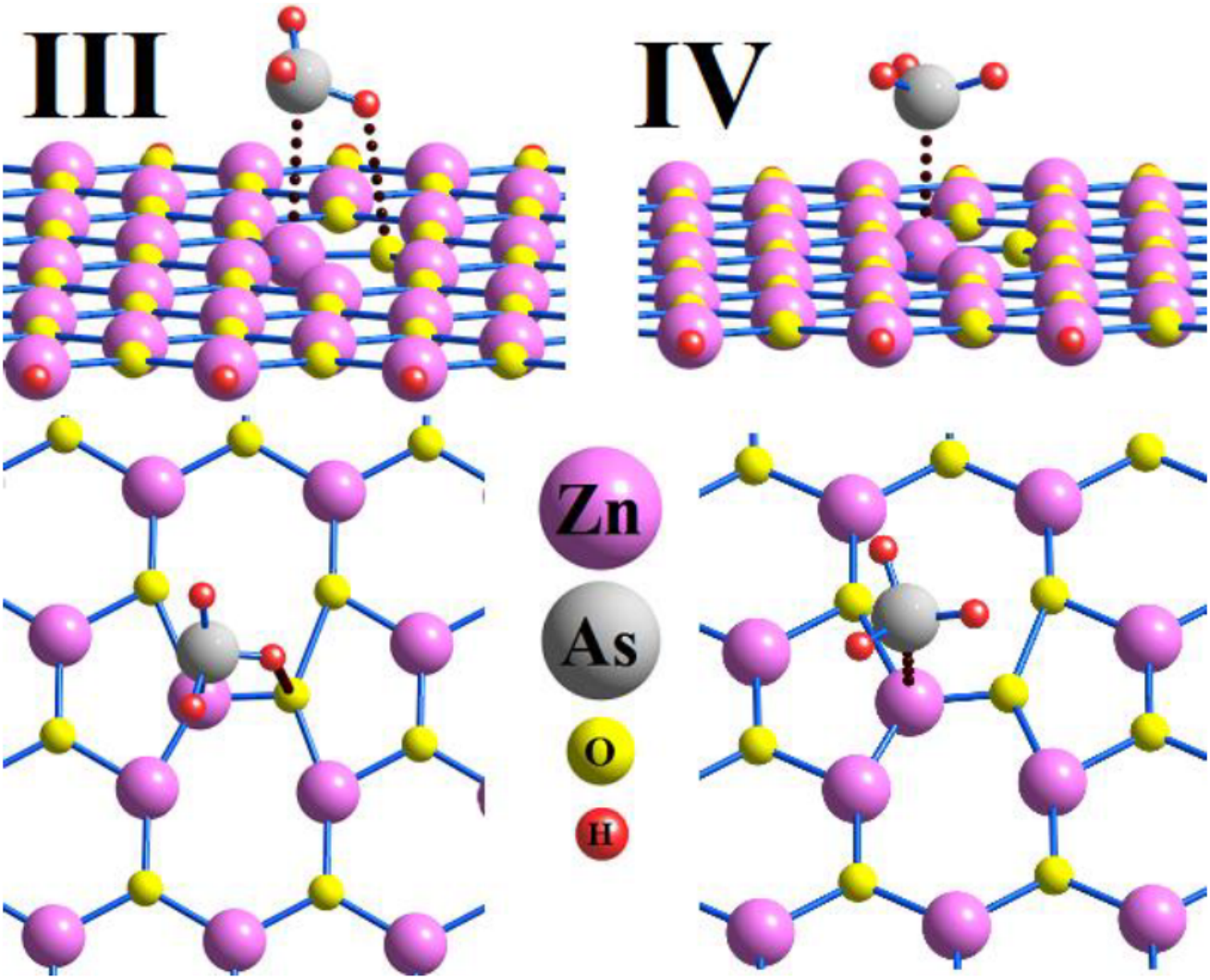

Figure 6

Optimized structure of AsH3/SW ZnO nanosheet complexes.

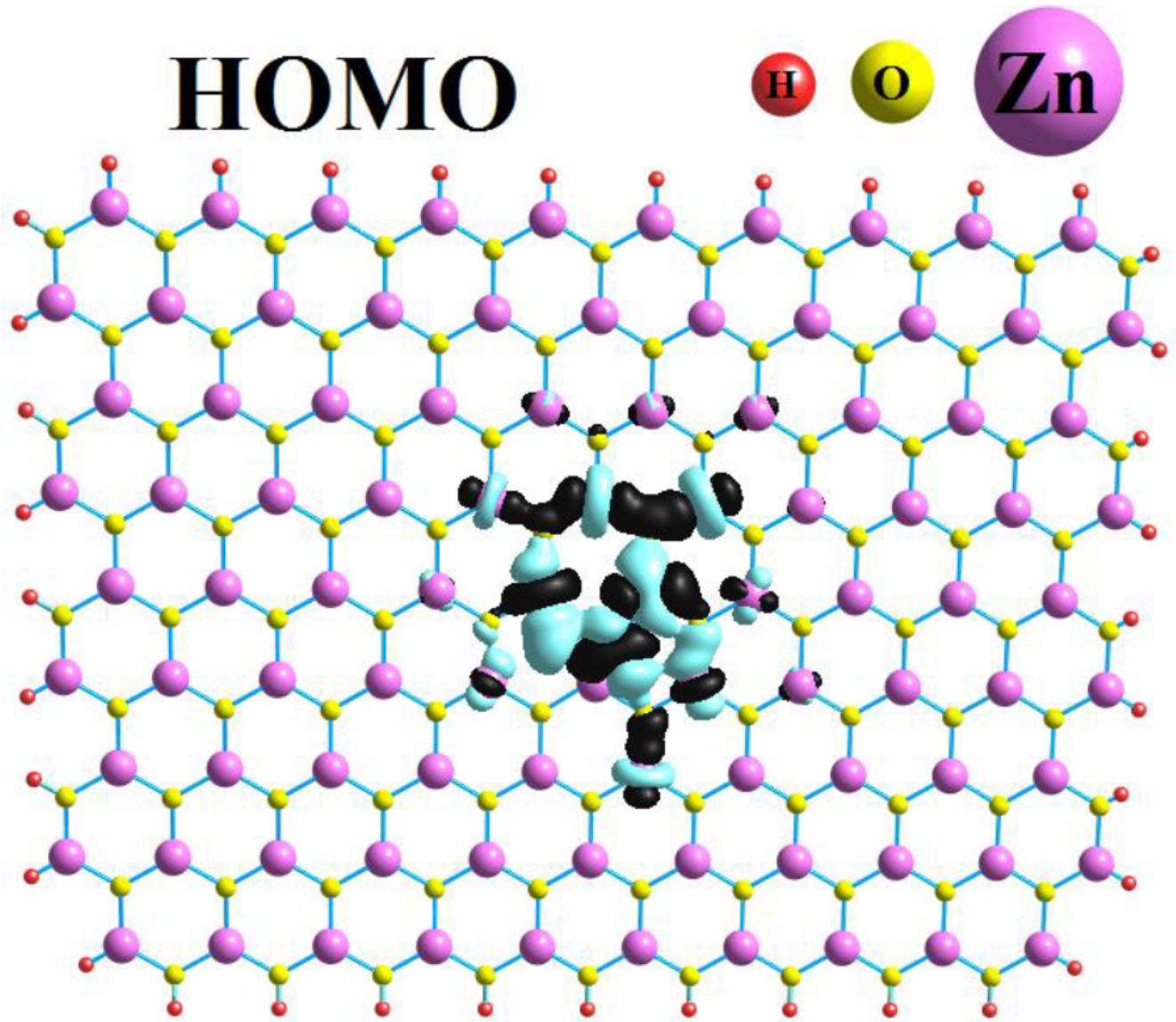

Figure 7

Partial density of states of the most stable AsH3/SW ZnO nanosheet complex and its HOMO profile.

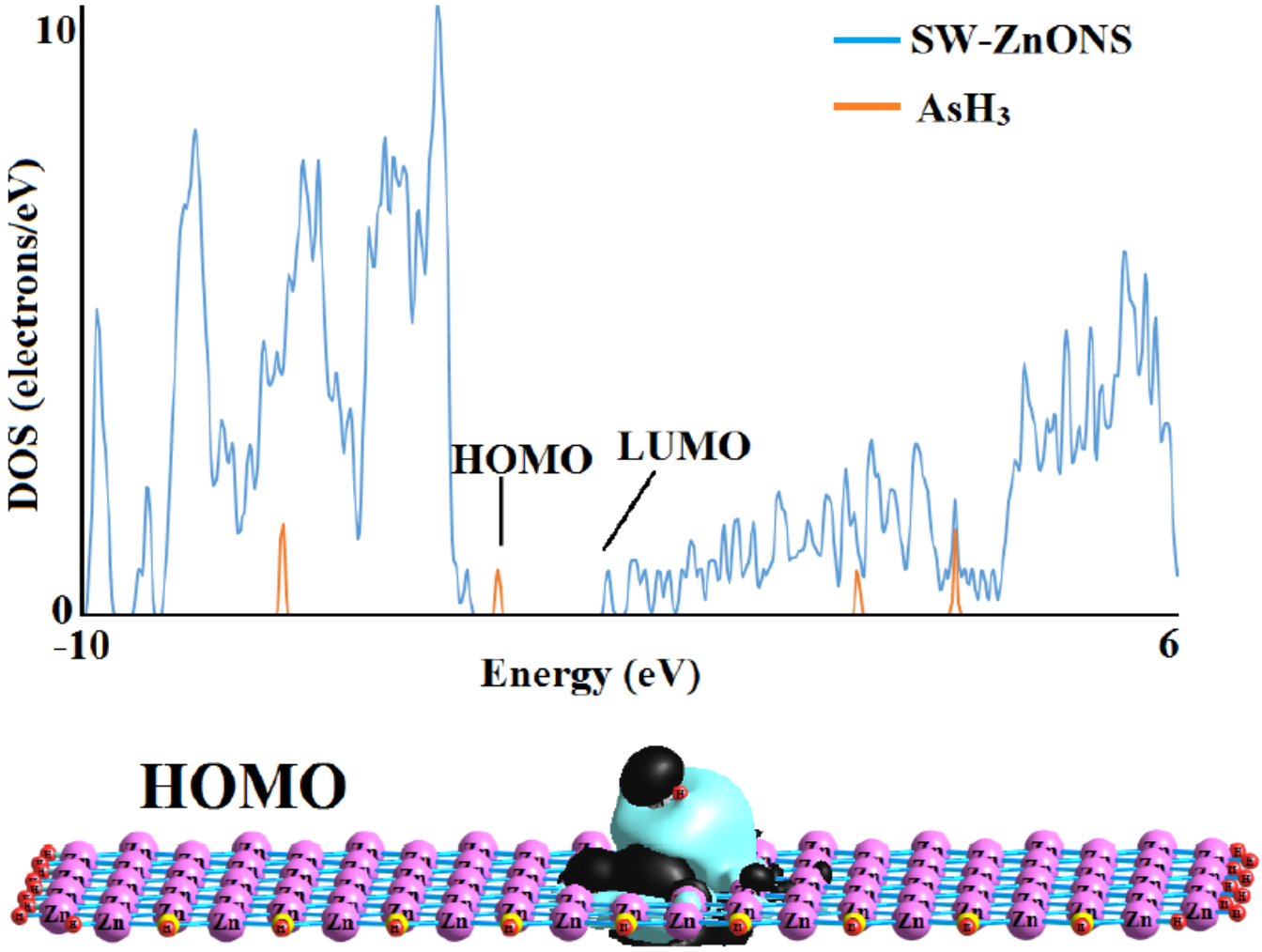

Figure 8

The HOMO profile of the Stone-Wales ZnO nanosheet complex.